OPEN ACCESS

University of BRISTOL

Cooper, G. A., Cobbin, M. R., & Ashfold, M. N. R. (2020). Effects of Ring Fluorination on the Ultraviolet Photodissociation Dynamics of Phenol. *Journal of Physical Chemistry A*, *124*(47), 9698-9709. https://doi.org/10.1021/acs.jpca.0c08927

Peer reviewed version

Link to published version (if available):
10.1021/acs.jpca.0c08927

Link to publication record in Explore Bristol Research
PDF-document

This is the author accepted manuscript (AAM). The final published version (version of record) is available online via ACS at https://doi.org/10.1021/acs.jpca.0c08927. Please refer to any applicable terms of use of the publisher.

University of Bristol - Explore Bristol Research
General rights

This document is made available in accordance with publisher policies. Please cite only the published version using the reference above. Full terms of use are available:
http://www.bristol.ac.uk/red/research-policy/pure/user-guides/ebr-terms/

Effects of Ring Fluorination on the Ultraviolet Photodissociation Dynamics of Phenol

Graham A. Cooper,*[†] Mackenzie R. Cobbin, and Michael N.R. Ashfold*

School of Chemistry, University of Bristol, Bristol, BS8 1TS, U.K.

*Authors to whom correspondence should be addressed

[†]Present Address: Department of Chemistry, University of Missouri, 601 S College Ave, Columbia, MO 65211, USA

Abstract

The dynamics of photoinduced O–H bond fission in five fluorinated phenols (2-fluorophenol, 3-fluorophenol, 2,6-difluorophenol, 3,4,5-trifluorophenol, and pentafluorophenol) have been investigated by H Rydberg atom photofragment translational spectroscopy following excitation at many wavelengths in the range $220 \leq \lambda \leq 275$ nm. The presence of multiple fluorine substituents reduces the efficiency of O–H bond fission (by tunneling) from the first excited ($1^1\pi\pi^*$) electronic state, whereas all bar the perfluorinated species undergo O–H bond fission when excited at shorter wavelengths (to the $2^1\pi\pi^*$ state). As in bare phenol, O–H bond fission is deduced to occur by non-adiabatic coupling at conical intersections between the photoprepared 'bright' $\pi\pi^*$ states and the $1^1\pi\sigma^*$ potential energy surface. In all cases, the fluorophenoxyl photoproducts are found to be formed in a range of vibrational levels, all of which include an odd number of quanta (typically one) in an out-of-plane (a'') vibrational mode; this product vibration is viewed as a legacy of the parent out-of-plane motions that promote non-adiabatic coupling to the dissociative $1^1\pi\sigma^*$ potential. The radical products also show activity in in-plane vibrations involving coupled (both in- and out-of-phase) C–O and C–F wagging motions, which can be traced to the impulse between the recoiling O and H atoms and, in detail, are sensitive to the presence (or not) of an intramolecular F···H–O hydrogen bond. Upper limit values for the O–H bond dissociation energies are reported for all molecules studied apart from pentafluorophenol.

1. Introduction

As the chromophore of the amino acid tyrosine, the response of phenol (PhOH) to ultraviolet (UV) irradiation has long been seen as important for our understanding of biological photochemistry. It is theorized that the photostability of tyrosine arises, in part, from the availability of an excited state relaxation channel in the phenol moiety wherein O–H bond extension facilitates non-radiative decay back to the ground state.[1-4] This bond extension and complete O–H bond fission in such molecules has thus been the subject of extensive study, both experimentally[5-21] and computationally.[1, 22-33]

Experimental studies have shown that the photodissociation of phenol following excitation at wavelengths λ ~270 nm proceeds via excitation from the ground electronic state, S_0, to the first excited singlet state, S_1, which has $^1\pi\pi^*$ character in the Franck-Condon (FC) region. The molecule then internally converts to the S_2 state, which has substantial 3*s* Rydberg character in the FC region but, on extension along the O–H bond coordinate ($R_{O–H}$), develops into a dissociative $^1\pi\sigma^*$ state. Figure 1 shows schematic cuts through these potential energy surfaces, along $R_{O–H}$, for planar geometries. When phenol is excited at wavelengths (λ) shorter than ~248 nm, the molecule has sufficient energy to couple through the S_2/S_1 conical intersection (CI). At longer wavelengths, however, close to the $S_1 \leftarrow S_0$ origin (λ ~275 nm), dissociation instead proceeds by tunneling through the barrier under this CI.[13, 14] Recent time-resolved studies have suggested that excitation of specific vibrational modes in the S_1 state molecule can increase this tunneling rate, although there remains some disagreement as to which modes lead to the largest rate enhancements.[18, 20] In Figure 1 and in the following discussion, we maintain consistency with the labelling scheme used in several previous studies for the electronic states of phenol, wherein the labels S_1, S_2, and S_3 are treated as synonymous with, respectively, the diabatic $1^1\pi\pi^*$, $1^1\pi\sigma^*$, and $2^1\pi\pi^*$ state descriptors.[7] This runs counter to the more traditional use of labels like S_n as adiabatic state descriptors. The two approaches return equivalent state labels in the FC region, but not at extended $R_{O–H}$ bond lengths.

Previous studies have also investigated how a variety of substituents on the phenyl ring affect the photoinduced O–H bond fission.[2, 3, 10, 13, 15, 34-40] Here, we explore how selective fluorination of the ring affects photoinduced O–H bond fission in phenol, both in terms of the number and position of fluorine atoms. The effect of multiple fluorination of aromatic molecules, culminating in the

perfluoro effect, has been the subject of research interest for many years.[41-46] The changes upon progressive fluorination of aromatic molecules manifest, among other ways, in the loss of detailed structure in UV absorption spectra,[42] in the reduction of fluorescence yields alongside shortened lifetimes,[43, 45] and, in the case of phenol, in a significant increase in acidity.[44] One of the fundamental changes contributing to these effects is the preferential stabilization of σ orbitals relative to π orbitals by multiple fluorine substituents.[41] In pentafluorophenol (PFP), this leads to low-lying $^1\pi\sigma^*$ states with C–F σ* character, which may fundamentally change the response of the molecule following absorption of UV light.[45]

This paper reports new H Rydberg Atom Photofragment Translational Spectroscopy (HRA-PTS) results following photoexcitation of several different fluorophenols at many different UV wavelengths in the range $220 \leq \lambda \leq 275$ nm and draws comparisons between these molecules and with bare phenol itself. To study the effects of substituent location, the photodissociations of 2- and 3-fluorophenol (2FP and 3FP respectively) have been investigated, and results compared with existing data on 4-fluorophenol (4FP).[34, 37] The effects of increased fluorination have then been probed by recording HRA-PTS spectra for 2,6-difluorophenol (26DFP), 3,4,5-trifluorophenol (345TFP), and pentafluorophenol (PFP). The structures of these molecules are all shown in the lower part of Figure 1. As in the original HRA-PTS studies of bare phenol,[7] analysis of the new data suggests that – in all cases – the radical fragments resulting from O–H bond fission are formed in levels with *a″* vibrational symmetry. Such energy disposal has been rationalized previously by assuming the product vibration to be a legacy of the parent nuclear motion (of *a″* symmetry) required to promote non-adiabatic coupling between the optically bright $1^1\pi\pi^*$ or $2^1\pi\pi^*$ states (both of which have $^1A'$ electronic symmetry) and the dissociative $1^1\pi\sigma^*$ state (with $^1A''$ electronic symmetry), but a complete understanding of this dissociating dynamics remains an ongoing challenge.[33]

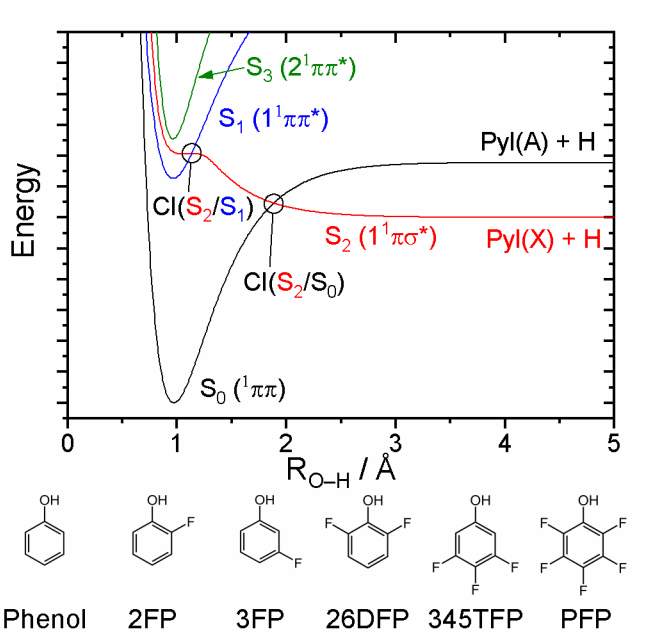

Figure 1 – Top: Schematic representation of cuts through the diabatic potential energy surfaces of the ground and first few excited singlet states of phenol along the O–H stretching coordinate, $R_{O–H}$. The crossings which develop into conical intersections when motion in other dimensions is considered are indicated. Bottom: Structures of phenol and the fluorophenols studied in this work.

2 Methods

2.1 Experimental methods

The HRA-PTS apparatus has been described in depth previously,[47, 48] and therefore only a brief summary, and the details specific to these experiments, will be recounted here. Samples of PhOH, PFP (both ≥99% purity), 2FP, 3FP, and 26DFP (all 98% purity) were purchased from Sigma-Aldrich, while 345TFP (97%) was acquired from Fluorochem. The compounds are all either liquids (2FP and 3FP) or low melting-point solids (PhOH, 26DFP, 345TFP, and PFP). In order to seed these molecules in a molecular beam, a sample of the solid, or of glass wool soaked in the liquid, was enclosed in a reservoir and heated (to between 30 and 70°C, depending on the molecule) to ensure a sufficient vapor pressure. Argon gas at a pressure of 1 bar (for solids) or 2 bar (for liquids) was passed through this reservoir and into the vacuum chamber using a pulsed valve (General Valve Series 9). The resulting jet was skimmed to create a molecular beam in the interaction region.

The target molecule was then dissociated using the frequency-doubled output from a tunable dye laser in the 220–275 nm wavelength range, and the resulting hydrogen atoms excited to high-lying Rydberg states (with principal quantum number, n ~80) using a 1 + 1' photoexcitation process comprising one photon at the Lyman-α wavelength (λ = 121.6 nm), followed by a second photon with λ ~364.6 nm. Those Rydberg-tagged atoms which recoil in the appropriate direction travel along a drift tube to the detector after passing through an electrical field (~50 V cm^{-1}) to remove any ions which are formed. Once these atoms pass through the grounded grid positioned close in front of the detector, they are field-ionized and the resulting protons are detected by a pair of microchannel plates, and their times-of-flight (TOFs) recorded. The distance between the interaction region and the detector (~0.61 m) was determined precisely by measuring H atom TOF spectra from the well-characterized photodissociation of H_2S in this same wavelength range,[49] thereby allowing determination of the H atom velocities and, by momentum conservation, the total kinetic energy release (TKER). All spectra were recorded with the polarization of the photolysis laser radiation perpendicular to the detection axis (the default orientation for the photolysis laser). Signal-to-noise ratio limitations prevented reliable measurement of recoil velocity anisotropy data.

2.2 Computational methods

The ground state equilibrium structures and vibrational wavenumbers of the molecules of current interest and of the radicals formed by O–H bond fission, and the parent O–H bond dissociation energies, were calculated at the density functional theory (DFT) level[50, 51] using the B3LYP functional[52-54] and Dunning's aug-cc-pVTZ basis set.[55-57] When determining the strength of O–H···F hydrogen bonding, and calculating vibrational constants for 2FP and 26DFP where such intramolecular bonding is relevant, Grimme's dispersion correction with Becke-Johnson damping was used.[58] All calculations were carried out using the Gaussian 09 software package.[59]

3 Results and Discussion

3.1 Electronic absorption spectra

Room temperature UV absorption spectra were recorded for PhOH, 2FP, 3FP, 26DFP, 345TFP, and PFP in cyclohexane solution, and are shown in Figure 2. All show an obvious absorption band at wavelengths ~260–280 nm, which gives way to a region of almost zero absorbance at ~240 nm

in all molecules except PFP followed, in all cases, by another region of strong absorption peaking at ~220 nm. The two strong absorption features in phenol are traditionally associated with excitation to the $1^1\pi\pi^*$ and $2^1\pi\pi^*$ states, respectively, both of which can predissociate by coupling to the $^1\pi\sigma^*$ continuum. The spectra for PhOH and PFP shown in Figure 2 are similar to the room temperature vapor phase spectra reported by Karmakar et al.,[45] and show the same pronounced differences upon perfluorination.

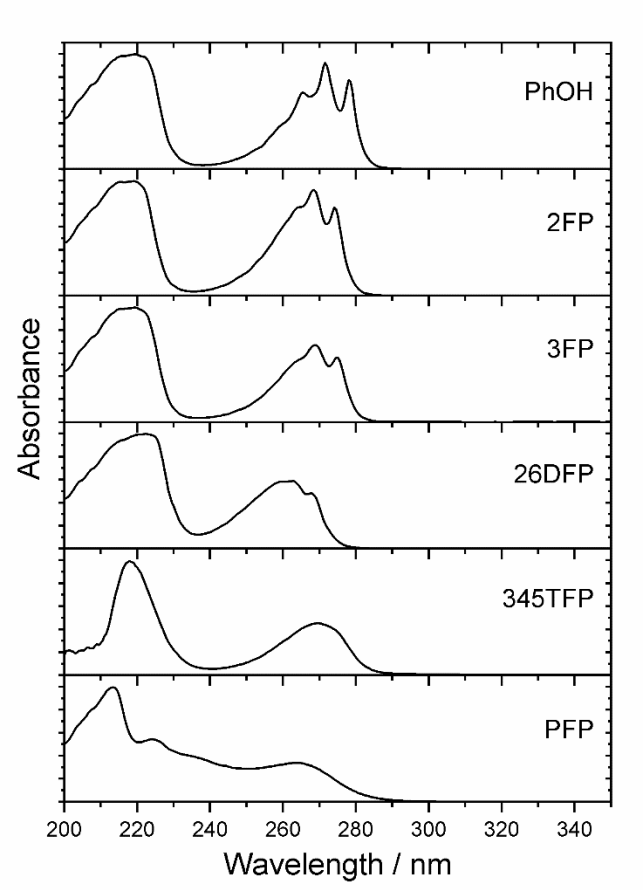

Figure 2 – UV absorption spectra recorded for phenol (PhOH), 2-fluorophenol (2FP), 3-fluorophenol (3FP), 2,6-difluorophenol (26DFP), 3,4,5-trifluorophenol (345TFP), and pentafluorophenol (PFP) in cyclohexane solution

Even at room temperature, the long wavelength feature in the absorption spectrum of phenol shows pronounced vibronic structure (which sharpens further into resolvable rovibronic features in the jet-cooled gas phase spectrum[60]), but these peaks become less sharp as the number of fluorine substituents increases and eventually disappear in 345TFP and PFP. This is consistent with the

reported loss of structure in the gas phase absorption spectra of benzene under increasing fluorination[42] and, in part, likely reflects the increase in spectral congestion that accompanies the increasing number of, and activity in, low frequency vibrational modes, although the recent study of PFP suggests that the congestion is exacerbated by the presence of additional intensity associated with the $^1\pi\sigma_{C-F}^*$ excited states.[45] Such behavior is similar to that found for the fluorobenzenes ($C_6F_nH_{6-n}$), where the energies of $^1\pi\sigma_{C-F}^*$ excited states are deduced to become comparable to (or even below that of) the lowest $^1\pi\pi^*$ state once $n \geq 5$.[43]

3.2 Effect of position on O–H bond fission in singly fluorinated phenols

To explore the effects of fluorination, it is useful to disentangle differences which result from changes to the electronic structure of the aromatic system due to the stabilization of σ* orbitals by the introduction of fluorine, from those which result from other causes. Specifically, it is possible for fluorine atoms in the ortho position to form intramolecular hydrogen-bonds with the hydroxyl group, and, to determine whether this inhibits photodissociation, the HRA-PTS spectra of 2FP and 3FP were compared. In chlorophenol, for example, the strength of intramolecular H-bonding (in the S_0 state) leads to an O–H bond dissociation energy in the ortho-isomer that is >400 cm^{-1} greater than that in the meta-isomer, despite the greater resonance stabilization of the ortho-radical product (as evidenced by analogous studies of the para-isomer).[40]

The photodissociation dynamics of 3FP (and 4FP) have been studied by HRA-PTS,[37, 39] but previous attempts to conduct such experiments on 2FP were unsuccessful. A recent publication by Deng et al., however, suggests that both 3FP and 2FP exhibit photofragmentation dynamics reminiscent of those of bare phenol, including an essential rôle for tunneling in dissociation from low-lying S_1 levels.[61] In what follows, these data are discussed first, before progressing through the increasingly fluorinated parents. TKER spectral assignment was guided by knowledge of the calculated wavenumbers (with anharmonic corrections) of all vibrational modes of each of the ground state parent molecules investigated, and the corresponding ground state radical fragments formed upon O–H bond fission. The results of these calculations are available in Tables S1 – S9 in the Supplementary Information (SI).

3.2.1 3-Fluorophenol

HRA-PTS spectra from dissociation of 3FP were recorded following excitation both at energies within the $S_3 \leftarrow S_0$ absorption (in the 220–230 nm range), well above the S_2/S_1 CI, and on individual vibronic peaks within the previously-observed $S_1 \leftarrow S_0$ resonance-enhanced multiphoton ionization (REMPI) spectrum.[39] A selection of these TKER spectra are shown in Figure 3, and the remainder are collected in Figure S1 in the SI. All the spectra show a broad, smooth feature rising at low kinetic energies. Such signals have been observed in many previous experiments involving a range of polyatomic hydrides and are generally attributed to processes where the electronically excited parent internally converts to vibrationally hot S_0 levels and then loses an H atom, or to processes involving multiple photons.[7, 11, 21, 34, 40, 47, 48, 62-64] Of greater current interest, the spectra also show a number of well-resolved peaks at higher TKER values, the positions and relative intensities of which vary with the photolysis wavelength. For completeness, we note that the TKER spectra recorded at the longest excitation wavelengths (i.e. when exciting low vibronic levels in the S_1 potential well) also show a weak tail extending to much higher kinetic energies, consistent with unintended resonance enhanced two photon excitation via these S_1 levels and subsequent dissociation, as observed previously in other phenols with relatively long-lived S_1 states.[7, 39, 61]

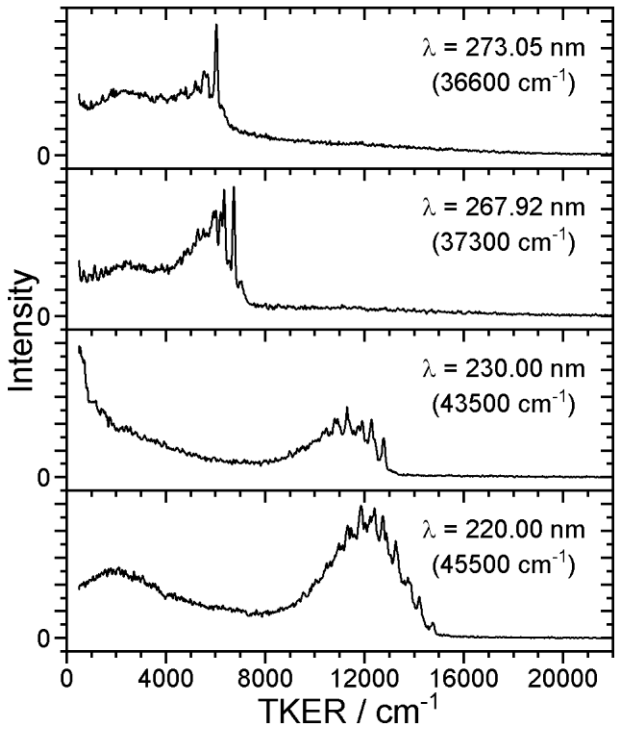

Figure 3 – Total Kinetic Energy Release spectra derived from H atom TOF spectra measured following photodissociation of 3-fluorophenol at the indicated wavelengths.

To aid comparison, it is helpful to transform spectra recorded at different photon energies into internal energy space using equation 1:

$$E_{\text{int}} = h\nu - \text{TKER} - D_0(\text{O–H}), \qquad (1)$$

where E_{int} is the internal energy of the 3-fluorophenoxyl (3FPyl) co-fragment, $h\nu$ the photon energy, and D_0(O–H) the dissociation energy of the O–H bond which in initial analyses is estimated, then refined to a value consistent with the experimental evidence. The internal energy in the jet-cooled parent molecule is (implicitly) assumed to be negligible. Plotting spectra using this transformed scale ensures that peaks corresponding to products in the same vibrational state align vertically, allowing for simple comparison. Figure 4 shows E_{int} spectra obtained following excitation on three peaks in the 1+1 REMPI spectrum of 3FP and two exemplar spectra at shorter wavelengths, calculated using the D_0(O–H) value determined below.

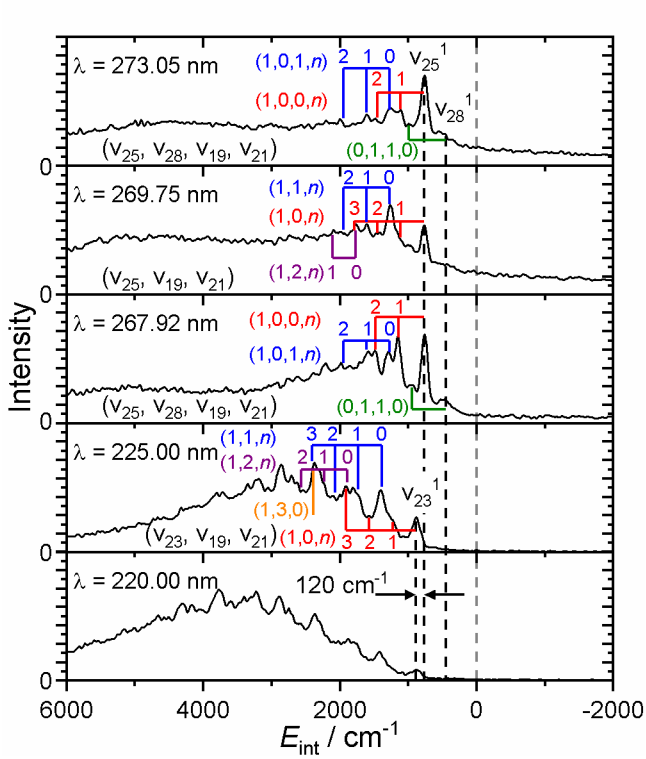

Figure 4 – HRA-PTS spectra from the photodissociation of 3-fluorophenol at the indicated wavelengths, plotted on an internal energy scale. The conversion from TKER to E_{int} was performed assuming D_0(3FPyl–H) = 29836 cm^{-1}. Combs indicate the assignment of peaks to vibrational modes of the 3-fluorophenoxyl radical labelled in Herzberg notation, with dashed vertical black lines drawn to highlight the energies of the different *a″* modes populated in the radical products formed at the different wavelength regions and the dashed vertical gray line to highlight the absence of radical products with E_{int} = 0.

3-Fluorophenol exists as a mixture of two conformers, *syn* and *anti*, which differ according to whether the hydroxyl bond is oriented, respectively, towards or away from the fluorine atom.[65-68] Spectra were recorded when exciting at the $S_1 \leftarrow S_0$ origin band of each conformer, and the difference in internal energy between corresponding product peaks found to be smaller than the peak widths. Furthermore, at shorter wavelengths, there is no discernible separation into peaks corresponding to the two parent conformers. The energy difference between the different conformers in the S_0 state is thus assumed to be negligible for the purposes of this work – consistent with MP2 estimates from Moreira et al.[66] which suggest an energy splitting less than ~70 cm^{-1} (i.e. within the peak widths in the TKER spectra shown in Fig. 4).

The spectra in Figure 4 closely resemble those published previously[39] (except for a reported spectrum at a photolysis wavelength of 270.67 nm, which could not be reproduced in the present

study) but show improved resolution which allows more detailed analysis. The main insight provided by the present spectra is that the peaks observed at the highest TKER (lowest E_{int}) in the short and long wavelength spectra do not correspond to the same product states, as previously assumed. As Figure 4 shows, these peaks fall at similar, but discernibly different, E_{int} values. Thus we conclude that the fastest H atoms formed by photolysis within at least one wavelength region (i.e. within either the long or short wavelength absorption bands) must be partnered by 3-fluorophenoxyl (3FPyl) radicals that are not in their ground vibrational states – mimicking findings from previous photofragmentation studies of phenol and its derivatives, where the phenoxyl products were found to be formed in states carrying an odd number of quanta in out-of-plane vibrational modes.[7, 34] Dixon et al. have discussed how activation of such out-of-plane (a'') vibrational motion in the radical product derives from the symmetry requirements accompanying non-adiabatic coupling between at the $S_2(^1A'')$ and $S_1(^1A')$ states at the S_2/S_1 CI,[14] but the detailed mechanism(s) underpinning this energy disposal remain a topic of intense theoretical research.[33]

In phenol and several para-substituted derivatives, the out-of-plane motions identified in the products formed when exciting at energies below and above the S_2/S_1 CI are the modes labelled 16a and 16b [7, 34, 64] (in Wilson notation[69]). Data on asymmetrically substituted phenols are more limited, as previous studies did not resolve an E_{int} difference in the products formed when exciting in the two wavelength regimes – reflecting inadequate experimental resolution, or that one parent mode could provide the dominant inter-state coupling in both regimes.[39, 40, 64]

By fitting the highest TKER peaks from the long- and short-wavelength spectra (ignoring, for now, the weak peaks seen at E_{int} ~450 cm^{-1} in some of the former), the separation between these hitherto unresolved peaks is ~120 cm^{-1} – as shown by the difference (indicated by the horizontal arrows) between the dashed vertical black lines aligned through the centers of the respective peaks in Figure 4. Comparing with the wavenumbers listed in Table S3, this ~120 cm^{-1} interval is seen to match well with the difference between radical modes ν_{23} (889 cm^{-1}) and ν_{25} (771 cm^{-1}) (in Herzberg notation[70]), both of which involve out-of-plane wagging of the C–H bonds and are orthogonal to the O–H stretch coordinate. The corresponding parent modes are ν_{25} and ν_{27} (with ground state wavenumbers of 878 cm^{-1} and 769 cm^{-1}, see Table S1) and the present data hint that the former motion may be the more effective at promoting non-adiabatic coupling when approaching the S_2/S_1 CI from higher energy whereas motion in S_1 state parent mode ν_{27} may be

more beneficial for tunneling through the barrier beneath it. These and other assigned radical modes are shown in Figure S2. One other feature of the spectra shown in Figure 4 merits note – namely the tail of signal intensity evident at nominally negative E_{int} values in spectra obtained at long excitation wavelengths, which is absent in the spectra recorded at short excitation wavelengths. Such tails correspond to very high TKER fragments, such as are formed by two photon excitation processes – which show with greatest probability in the cases of molecules with long-lived, resonance enhancing S_1 states. The non-observation of any such signal at TKERs greater than permissible by one photon energy conservation when exciting at short wavelengths implies that non-adiabatic coupling following photoexcitation of the S_3 state is efficient and fast.

The improved energy resolution of the present experiments also allows detection and identification of weaker peaks in the TKER spectra recorded at longer excitation wavelengths, including one associated with H-atoms travelling slightly faster than those associated with co-fragments in the $v_{25} = 1$ state. The E_{int} value of the peak that is most obvious in the spectrum taken at $\lambda = 267.92$ nm matches well with that of the out-of-plane radical mode ν_{28} (425 cm^{-1}), hinting that the corresponding parent motion (v_{30}) may also help promote tunneling through the barrier beneath the S_2/S_1 CI. Such would not be unprecedented: previous phenol photodissociation studies identified similar weak features corresponding to a second radical mode of a'' symmetry that could plausibly indicate the operation of a second parent coupling mode.[7]

The remainder of the peaks in the HRA-PTS spectra shown in Figures 4 and S1 can be assigned to combination bands involving one quantum of the a'' product mode in combination with different numbers of quanta in in-plane modes ν_{19} (501 cm^{-1}) and ν_{21} (342 cm^{-1}), as illustrated by the combs arranged above the longer wavelength spectra in Figure 4. These two modes are, respectively, the in- and out-of-phase in-plane wagging motions of the C–O and C–F bonds, as shown in Figure S2, which are logically activated by the recoil of the departing H atom on the pendant O atom. More extensive progressions in these in-plane modes are seen in the spectra recorded at shorter wavelengths, consistent with an increased impulse; sample assignments are shown for the spectrum recorded at $\lambda = 225$ nm. Peak assignments at high E_{int} become ambiguous, however, since the energy of two quanta of ν_{19} (~1002 cm^{-1}) or three quanta of ν_{21} (~1026 cm^{-1}) are very similar. Because of this increased spectral congestion, higher energy peaks are not assigned in

Figure 4, though all of the major features can be assigned (albeit not uniquely) to various combinations of these two modes built on a quantum of *a″* vibration.

Having assigned these features, it is possible to derive an O–H bond strength for 3-fluorophenol, D_0(3FPyl–H) = 29840 ± 50 cm^{-1}, slightly lower than the previously published value due to the reassignment of the various product features.[39] Table 1 compares the experimentally determined O–H bond dissociation energies for this and other molecules studied in this work with the (zero-point corrected) values returned by the accompanying calculations.

Table 1 – Comparison of O–H Bond Strengths in Phenol and Fluorinated Phenols Determined by Analysis of HRA-PTS Data and by the Accompanying B3LYP/aug-cc-pVTZ Calculations (which Include Corrections for Basis Set Superposition Error and Changes in Zero-Point Energy). The Experimental Values may be Viewed as Upper Limits to the O–H Bond Strength (*vide infra*).

Molecule	D_0(O–H) / cm^{-1}	
	Experiment	Calculated
PhOH	30015 ± 40[a]	28870
2FP	30220 ± 50	29430
3FP	29840 ± 50	29130
26DFP	29510 ± 50	28890
345TFP	30100 ± 50	28730

[a]From Nix et al.[7]

3.2.2 2-Fluorophenol

Fluorination at the ortho and meta positions impact differently on the electronic structure of phenol, but a more significant distinction between 2FP and 3FP may be the ability of the former to form an intramolecular hydrogen bond. Though some prior studies have claimed that no such H-bond exists,[71, 72] there is significant evidence that it does – spanning computational work[73-75] and a range of experimental results such as shifts in infrared absorption peaks,[65] shortened interatomic distances found by microwave spectroscopy,[68] and an NMR study.[76]

This intramolecular H-bond is somewhat strained and therefore of reduced strength. Prior studies have suggested that the H-bond is weaker than that in 2-chlorophenol,[76, 77] and that 2FP prefers to form intermolecular H-bonds when possible in the solid phase,[78] in concentrated solutions,[66, 77] or in polar solvents.[66] However, the existence of the intramolecular bond still has some significant effects.

Like 3FP, 2FP can exist in *syn*- and *anti*-conformers, but the H-bond in 2FP causes a significant relative stabilization of the *syn*-conformer. Though some earlier studies suggested that both conformers co-exist, at least in the vapor phase,[79-81] more recent hole-burning experiments have shown that peaks that hitherto had been assigned to *anti*-2FP are in fact from the *syn* form,[82] and further experiments and energetic arguments suggest that only the H-bonded conformer may be present under molecular beam conditions.[83] The present B3LYP-D3BJ/aug-cc-pVTZ calculations suggest that the ground state *syn* conformer is more stable by ~900 cm^{-1}, consistent with previous values of ~1000 cm^{-1} found at the MP2 level.[66, 73]

The intramolecular H-bond can be expected to impact on the O–H bond dissociation dynamics, both by stabilizing the parent molecule and by directly impeding loss of the hydrogen atom. Photoinduced O–H bond fission in the 2-chlorophenol analogue was only observed at higher photon energies.[40] However, Deng et al. have shown that 2FP can dissociate (by tunneling) from low-lying S_1 levels although, relative to 3FP, they note that the S_1 lifetime is extended and that the one-photon-induced H-atom product yield is significantly reduced as 'the OH stretch motion promoting the tunneling process is restricted' by the H-bonding.[61]

In this study, we succeeded in recording TKER spectra from photodissociation of 2FP in two different wavelength regions: at energies within the $S_3 \leftarrow S_0$ absorption, at total energies well above the S_2/S_1 CI, and when exciting low-lying S_1 levels identified in previous spectroscopic studies[82, 83] – from which any excited state O–H bond fission must involve tunneling through the barrier beneath this CI. These spectra are shown as Figure S3 in the SI. As in the case of 3FP, the spectra show a broad, intense feature peaking at low TKER (attributable to the decay of parent molecules following radiationless transfer to vibrationally 'hot' S_0 levels). The feature extending to TKER values much greater than that allowed by a single-photon UV absorption process is also evident in all spectra recorded at long excitation wavelengths, and is relatively much stronger than in the case of 3FP – hinting at a significant contribution from resonance enhanced multiphoton excitations.

Similar multiphoton-induced signal has been recognized in velocity map imaging studies of 2FP photodissociation at λ ~271 nm and is not unexpected given the increased S_1 state lifetime (cf. 3FP).[61] Possible multiphoton excitation mechanisms have been considered, but not resolved, in a recent theoretical study.[84]

Again, the sharp features which show photolysis wavelength dependent TKERs and intensities are of greatest current interest. These are relatively much less intense that those in the corresponding spectra obtained from 3FP. Again, to aid comparison and assignment, the data were converted to an E_{int} scale. Figure 5 shows spectra obtained at wavelengths that match with several different transitions to low-lying S_1 levels observed and assigned by Yuan et al.,[83] along with two representative spectra taken when exciting to the S_3 state, at λ = 227.5 and 225 nm, i.e. at energies well above the S_2/S_1 CI. Again, we highlight the absence of signal at TKERs that can only arise via multiphoton processes in the spectra recorded at short excitation wavelengths (Figure S3) suggesting that, as in 3FP, the decay of 2FP(S_3) molecules is much quicker than that of 2FP(S_1) molecules.

As in 3FP, the peaks evident at low E_{int} (Figure 5) in spectra obtained by exciting 2FP in the long- and short-wavelength regions do not align to the same internal energy levels of the 2-fluorophenoxyl radical product but, in this case, the lowest energy feature in the E_{int} spectra recorded at longer excitation wavelengths has higher internal energy than the lowest energy feature in the E_{int} spectrum recorded at short wavelengths (indicated by the black and yellow vertical dashed lines, respectively, in Figure 5). The ~195 cm^{-1} energy mismatch in this case can be most readily accommodated by assuming that the peaks appearing at highest TKER in spectra recorded at long and short excitation wavelengths indicate population of, respectively, out-of-plane radical modes ν_{25} (766 cm^{-1}) and ν_{27} (553 cm^{-1}) – both of which are illustrated, along with the other lower energy out-of-plane radical modes, in Figure S4.

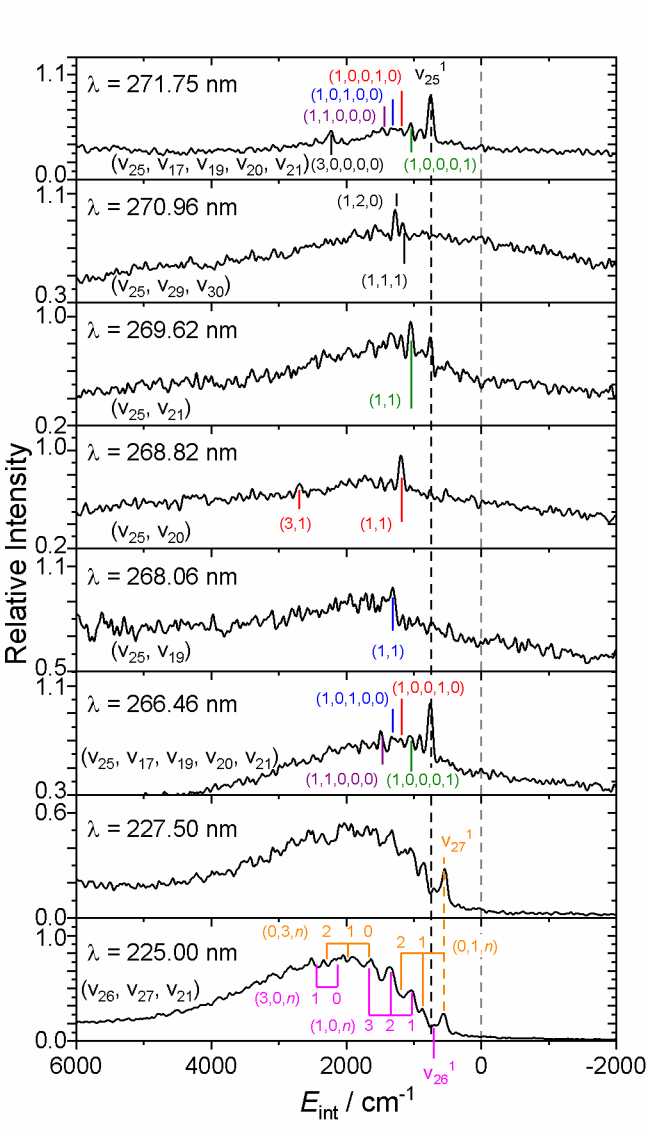

Figure 5 – HRA-PTS spectra from the photodissociation of 2-fluorophenol at the indicated wavelengths plotted on an internal energy scale. The conversion from TKER to E_{int} assumed D_0(2FPyl–H) = 30216 cm^{-1}. Lines and combs indicate assignments of peaks to vibrational modes of the 2-fluorophenoxyl radical labelled in Herzberg notation; the proposed assignments of features at E_{int} >1500 cm^{-1} in the λ = 225 nm spectrum are one (of several) plausible interpretations of the observed structure. The y-axes have been expanded where necessary to accommodate the high background signal intensity.

The parent analogue of 2-fluorophenoxyl (2FPyl) radical mode ν_{25} is ν_{27}, with a calculated (anharmonic) wavenumber of 749 cm^{-1} in the ground state (Table S4). The deduced population of this *a″* mode of the product hints that parent excited state mode ν_{27} – which involves very similar out-of-plane hydrogen wagging motions to the ν_{27} parent mode implicated in H atom loss

following excitation to the S_1 state of 3FP – may be particularly effective at promoting tunneling through the barrier under the S_2/S_1 CI. The spectrum recorded at λ = 271.75 nm (corresponding to excitation on the $S_1 \leftarrow S_0$ origin of *syn*-2FP) shows peaks consistent with population of levels with both one and three quanta of excitation in radical mode ν_{25}, in combination with four low-wavenumber, in-plane modes (illustrated in Figure S5): ν_{17} (a ring-breathing mode analogous to parent mode ν_{19}), ν_{19} (the in-phase C–O and C–F wagging mode, analogous to parent mode ν_{21}), ν_{20} (a ring distortion analogous to 2FP mode ν_{22}), and ν_{21} (the out-of-phase C–O and C–F wagging mode, descended from mode ν_{23}), although the signal-to-noise ratio of some of these peaks is quite low (reflecting the presumed lower primary dissociation yield (cf. 3FP)).

Upon tuning the photolysis energy to match that of a transition to an FC favored S_1 vibrational level, the resulting E_{int} spectrum consistently shows (at least some) enhanced intensity in the corresponding in-plane radical mode. For example, excitation at λ = 269.62 nm (assigned to the S_1, ν_{23}=1 ← S_0, v=0 transition, henceforth reported simply and more compactly as 23_0^1)[83] leads to an obvious enhancement of the peak assigned to radical mode ν_{25}=1 + ν_{21}=1 (henceforth abbreviated as $\nu_{25}^1\nu_{21}^1$). Similarly, excitations at λ = 268.82 nm (parent 22_0^1 transition), λ = 268.06 nm (21_0^1) and λ = 266.46 nm (19_0^1) result in obvious enhancements of features in the E_{int} spectra assigned to, respectively, $\nu_{25}^1\nu_{20}^1$, $\nu_{25}^1\nu_{19}^1$ and $\nu_{25}^1\nu_{17}^1$. This is classic 'spectator' mode behavior, as seen in bare phenol;[7, 10] in each case, the in-plane parent motion excited in the S_1 state maps through as the corresponding vibration in the radical (always in combination with a quantum of the *a″* mode ν_{25} that we assume is introduced via non-adiabatic coupling to the S_2 potential). The wavenumbers of ground state radical modes ν_{17}, ν_{19}, ν_{20}, and ν_{21} can be determined based on their appearance in multiple TKER (and E_{int}) spectra, and the average values so derived are included in Table S5 for comparison with the calculated values. The spectrum recorded at λ = 270.97 nm, when exciting the τ_0^2 torsion transition, is different. Remmers et al. identified that the torsion mode in question is most likely a butterfly mode, involving out-of-plane wagging of the C–O and C–F bonds.[82] The present HRA-PTS study returns weak peaks at E_{int} values corresponding to ν_{25}=1 in combination with both ν_{29}^2 and with $\nu_{29}^1\nu_{30}^1$. Radical modes ν_{29} and ν_{30} are, respectively, the in- and out-of-phase out-of-plane wagging modes of the C–O and C–F bonds. Both modes have *a″* vibrational symmetry, as does ν_{25}, so the overall product vibrational symmetry

is, again, *a″* – as required for conservation of vibronic symmetry in the non-adiabatic coupling from S_2 to S_1.

Clearly different behavior is observed when exciting 2FP at energies well above the S_2/S_1 CI. The E_{int} spectra are most logically assigned to short progressions in radical mode ν_{21} (the in-plane, out-of-phase C–O and C–F wagging mode) in combination with out-of-plane (*a″*) modes ν_{26} and ν_{27}. In contrast to 3FP, no substantial excitation of the corresponding in-plane, in-phase mode (ν_{19}) is observed when exciting at these shorter wavelengths. We surmise that this could be because the loss of the intramolecular H-bond (by photoinduced loss of the H atom) induces an impulse (in opposite directions) on both the O and F atoms (given their similar masses and similar bonding to their respective ring C atoms) that translates preferentially into the out-of-phase motion ν_{21} depicted in Figure S5.

The progressions built on the two different *a″* modes show some obvious differences. The $\nu_{27}^1\nu_{21}^n$ progression shows maximum intensity when $n = 0$ and declines steeply such that the $\nu_{27}^1\nu_{21}^2$ peak is hard to discern. The intensity distribution in the $\nu_{26}^1\nu_{21}^n$ progression, in contrast, increases until at least $n = 2$, with the fundamental (i.e. $\nu_{26}^1\nu_{21}^0$ peak) barely observable as a shoulder on the high E_{int} side of the ν_{27}^1 feature. These different behaviors likely reflect differences in the forces acting in the excited state of the parent molecule and in the region of the S_2/S_1 CI. However, a thorough theoretical treatment well beyond the scope of this work would be required to investigate and rationalize such multi-dimensional vibronic interactions.

The mutually self-consistent assignment of all HRA-PTS data for 2FP shown in Figures 5 and S3 allows determination of the O–H bond strength in 2-fluorophenol, D_0(2FPyl–H) = 30220 ± 50 cm^{-1} (listed in Table 1), which is ~380 cm^{-1} larger than that for 3FP (see section 3.2.1) and ~850 cm^{-1} higher than the corresponding value (29370 ± 50 cm^{-1}) for 4FP.[34] This ordering of the relative bond strengths matches that found for the corresponding monochlorinated phenols,[40] and reflects the net result of two competing effects. One is the resonance stabilization of the product radical by ortho- or para-substitution, which accounts for the lower D_0(O–H) value for 4FP compared with 3FP. The second, specific to 2FP, is the parent stabilization afforded by intramolecular hydrogen bonding. That 2FP exhibits the highest D_0(O–H) value implies that the energetic stabilization of the parent is greater than that provided by the resonance stabilization of the radical product. Thus the present experiments provide further

confirmation that there is an O–H···F hydrogen bond in 2FP and that it has discernible consequences both for the thermochemistry of the O–H bond fission process and for the parent tunneling probability and H-atom product yield when exciting to S_1 levels at energies below the S_2/S_1 CI – thereby lending support to the recent kinetic studies of this process by Deng et al.[61]

3.3 Effects of multiple fluorination

The photodissociation of three phenol derivatives containing multiple fluorine atoms was also studied. Of these, 2,6-difluorophenol has parallels with 2FP in as much that it exhibits similar intramolecular hydrogen bonding. 3,4,5-trifluorophenol does not, but simply illustrates the effects of increasing fluorination, while pentafluorophenol represents the culmination of the fluorination process and possesses the same intramolecular H-bonding opportunity as 26DFP and 2FP.

One obvious effect of multiple substitution is that excitation near the S_1–S_0 origin no longer yields structured HRA-PTS spectra. For all three molecules, such long wavelength photoexcitation results in weak, broad and structureless H atom TOF distributions. Much more intense H atom signals are observed when exciting both 26DFP and 345TFP at shorter wavelengths (λ ~225 nm), and the TOF spectra in both cases do show structure – as illustrated by the corresponding TKER spectra shown in Figures S6 and S7, respectively.

Figure 6 shows two sample spectra obtained following short UV wavelength photolysis of 26DFP, plotted on an E_{int} scale, with what we consider to be the most plausible peak assignments. As in the case of 2FP, these short wavelength spectra appear to display two progressions of peaks. The interval in each progression (~300 cm^{-1}) matches well with the calculated wavenumber for ν_{21}, the in-plane, out-of-phase C–O and C–F bending mode in the 2,6-difluorophenoxyl radical (shown in Figure S8) and, as in 2FP, we assume that this mode is preferred over its in-phase counterpart (ν_{17}) when energy is deposited into the radical upon removal of the O–H···F hydrogen bond. However, the wavenumber separation between the two progressions (~135 cm^{-1}) is too small to correspond to any in-plane vibrational mode of the radical and, again, analogy with 2FP leads us to propose that these progressions are each built on a quantum of (different) out-of-plane (a'') modes that derive from two different parent coupling modes. The assignment which fits the measured spectra best invokes radical modes ν_{23} and ν_{25} (two predominantly out-of-plane C–H bending modes, out-of-phase and in-phase respectively, also shown in Figure S8).

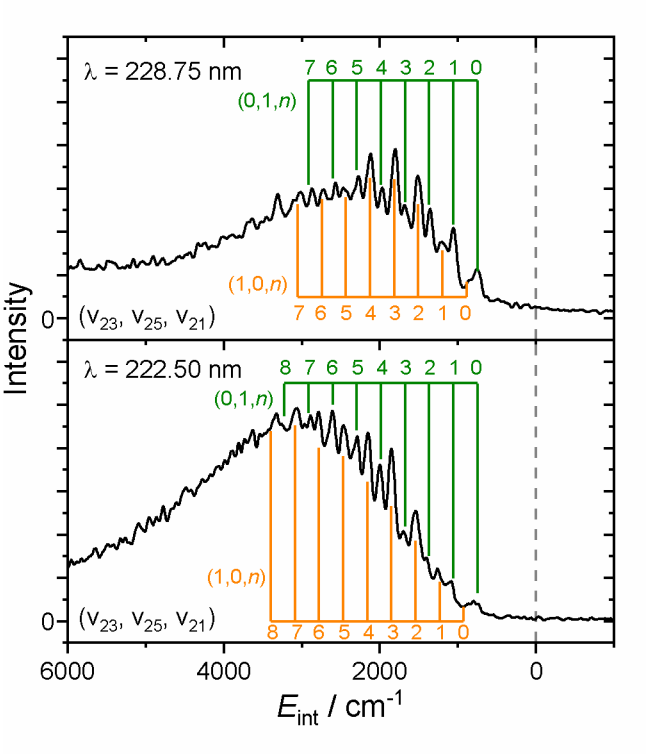

Figure 6 – HRA-PTS spectra from the photodissociation of 2,6-difluorophenol at the indicated wavelengths, plotted on an internal energy scale. The conversion from TKER to E_{int} assumed D_0(26DFPyl–H) = 29508 cm^{-1}. Lines and combs indicate assignment of peaks to vibrational modes of the 2,6-difluorophenoxyl radical labelled in Herzberg notation; for simplicity, the combs have been drawn assuming a constant energy separation between successive ν_{21}^n levels.

In a further similarity to 2FP, there are clear differences in the relative peak intensities within the $\nu_{23}^1\nu_{21}^n$ and $\nu_{25}^1\nu_{21}^n$ progressions. The former progression appears relatively weaker at low n, but becomes comparable (or greater) in magnitude at higher n – though the differences are less striking than in the case of 2FP.

The TKER of the peak assigned to formation of an H atom in conjunction with the 2,6-difluorophenoxyl (26DFPyl) radical in the ν_{25}^1 level, together with the calculated wavenumber of this level (752 cm^{-1}, Table S7), allows estimation of the O–H bond strength in 2,6-difluorophenol: D_0(26DFPyl–H) = 29510 ± 50 cm^{-1}. Table 1 shows that this experimental value again accords well with the calculated O–H bond strength. The reduction (cf. 2FP) can be readily understood in terms of additional stabilization of the radical by introducing another fluorine atom in the ortho-position. Table 1 also serves to illustrate the consistency between the

experimentally derived and computed O–H bond strengths in 2FP, 3FP, and 26DFP. The latter are consistently ~600 – 800 cm^{-1} lower than the experimentally derived quantities – a point to which we return later.

3,4,5-Trifluorophenol shows similarities and differences (cf. 26DFP) in its short wavelength photodissociation dynamics, as illustrated by the sample E_{int} spectra displayed in Figure 7. As in 26DFP, the TKER and E_{int} spectra are best interpreted in terms of progressions built on two out-of-plane modes (ν_{27} and ν_{28}, shown in Figure S9) with a wavenumber separation of just 80 cm^{-1}. Again, these modes involve, respectively, in- and out-of-phase C–H wagging motions, but with some significant ring puckering in both cases. In contrast to 26DFP, these two modes support progressions involving both ν_{15} and ν_{19} (the two in-plane C–O bending modes, in- and out-of-phase with the C–F bending motion, respectively, as also shown in Figure S9). Thus, as in 3FP, in the absence of intramolecular hydrogen bonding, both are excited, rather than just the latter. Given the multitude of possible combinations of quanta in these modes it becomes impossible to offer definitive assignments of the peaks apparent at E_{int} >1500 cm^{-1}, although all can be attributed to one or more of these progressions.

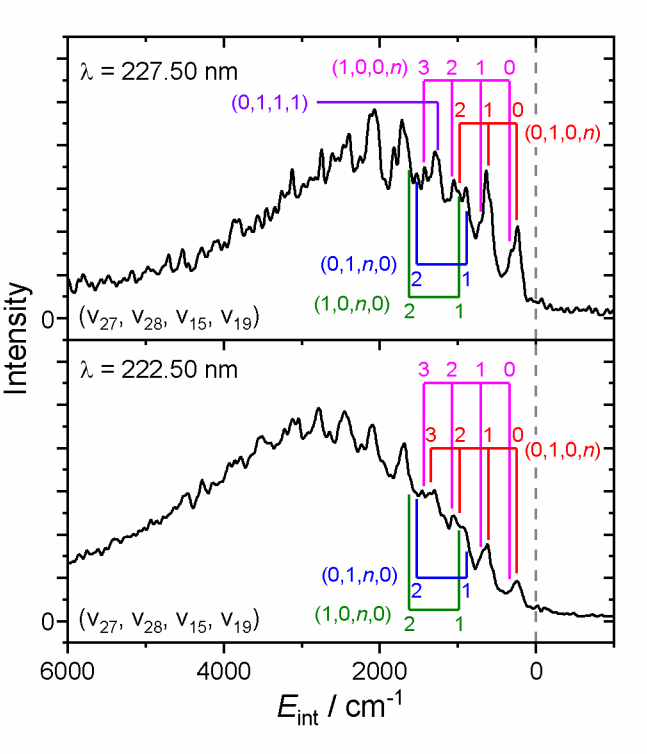

Figure 7 – HRA-PTS spectra from the photodissociation of 3,4,5-trifluorophenol at the indicated wavelengths, plotted on an internal energy scale. The conversion from TKER to E_{int} assumed D_0(345TPyl–H) = 30102 cm^{-1}. Lines and combs indicate assignment of peaks to vibrational modes of the 3,4,5-trifluorophenoxyl radical labelled in Herzberg notation.

The TKER of the peak assigned to formation of an H atom in conjunction with the 3,4,5-trifluorophenoxyl (345TFPyl) radical in the v_{28}^1 level, together with the calculated wavenumber of this level (570 cm^{-1}, Table S9), allows estimation of the O–H bond strength in 3,4,5-trifluorophenol: D_0(345TFPyl–H) = 30100 ± 50 cm^{-1}. This is similar to that in bare phenol[7] and higher than that found for the other fluorinated phenols – despite the lack of an intramolecular H-bond and the presence of a (potentially radical stabilizing) F atom in the para-position. As Table 1 shows, there is also a significantly larger difference (~1400 cm^{-1}) between the experimentally derived and computed O–H bond strength in 345TFP – roughly twice as large as the corresponding difference for the other fluorinated phenols, and larger than the corresponding difference for bare phenol (~1150 cm^{-1}), the other (minor) outlier in Table 1.

One possible cause for this discrepancy could be an incorrect assignment of the observed peaks. No peak associated with forming radical products in the v = 0 level is identified in any of the

spectra reported in this work, and in the case of 345TFP, the fastest features are assigned to H + 345TFPyl(ν_{27} = 1 or ν_{28} = 1) products. At higher E_{int}, stronger features are associated with excitation of ν_{19} built on these *a″* modes and, if the forces responsible for activity in these modes are sufficiently strong, it is possible that the features labelled by the pink and red combs in Figure 7 should be assigned to the ν_{19} = 1–4 progression (rather than 0–3 as indicated). Thus, whilst Figure 7 shows the assignment we consider most probable, it is not inconceivable that the true origin is shifted by one or more quanta of ν_{19} – which would have the effect of reducing the experimentally derived D_0(O–H) value by 367 cm^{-1} (or a multiple thereof).

In addition, the degree of rotational excitation in the radical products is uncertain. The peaks in the various E_{int} spectra are all quite narrow, implying that the radicals formed in any given vibrational state carry a rather small spread of rotational energies. Prior experimental analyses assumed that this narrowness implied that the radical products carried little rotational excitation,[7, 39] but a recent excited state non-adiabatic dynamics study employing the best available multi-dimensional potential energy surfaces for bare phenol suggests that the PhO radicals from PhOH photolysis at long wavelengths are formed in a narrow spread of high rotational energy levels.[33] None of the experiments reported to date have the resolution to confirm or refute this predicted energy disposal but, if correct and if applicable to the dynamics of substituted phenols induced by both short and long wavelength photolysis, then the experimentally derived D_0(O–H) values listed in Table 1 could over-estimate the true (i.e. parent and product rotation-free) value by 100 cm^{-1} or more. These possible uncertainties in both the vibrational and rotational assignments apply to the spectra of all of the molecules reported in Table 1 and, for these reasons, it is prudent to regard the experimentally derived D_0(O–H) values as upper limit values.

The ‘offsets’ between the lowest energy E_{int} peaks identified in TKER spectra recorded in the long and short wavelength regions – which we here ascribe to different population of different *a″* product states – could potentially instead be explained by invoking very different rotational energy disposals in the products. We regard this as most improbable, however, given (i) the very different amounts of product rotation that would be required to accommodate the observed energy offsets, (ii) the relative narrowness of the observed peaks, which implies consistently narrow spreads of rotational energy, (iii) the change in the sign of the energy offset deduced in the cases of 2FP and 3FP, and (iv) the very unusual bimodal rotational distributions that would be required in order to

explain the energy disposal in the products from short wavelength photolysis of 26DFP and 345TFP as distributions in a single vibrational mode.

Given the successful observation of H atoms attributable to O–H bond fission in each of the above fluorophenols, efforts were made to record similar spectra from UV photolysis of pentafluorophenol. The detected H atom yields at all investigated wavelengths were, however, small and the TOF spectra of these H atoms were devoid of any structure; the derived TKER spectra resemble broad humps, as illustrated in Figure S10. This finding casts doubt on the recent suggestion that O–H bond fission might be responsible for the much reduced fluorescence emission from PFP when exciting to progressively higher S_1 vibronic levels,[45] but would be consistent with the results of subsequent molecular dynamics simulations[46] which found that the S_2 and S_3 states of PFP (both of which are identified as $\pi\sigma^*$ states) are sufficiently lowered by perfluorination that they efficiently mix with the S_1 state and permit ultrafast redistribution between these states. The σ^* orbitals contributing to these states have dominant C–F character, and the resulting $^1\pi\sigma_{C-F}^*$ states are predicted to be bound. In light of this, the present experimental data suggest that, following photoexcitation, PFP molecules decay preferentially by non-adiabatic coupling to the S_0 state via one or more coordinates other than O–H bond extension and that the observed H atoms derive from the subsequent dissociation of a fraction of these vibrationally hot S_0 molecules.

4 Conclusions

The dynamics of O–H bond fission following UV photoexcitation of five fluorinated phenols (2- and 3-fluorophenol, 2,6-difluorophenol, 3,4,5-trifluorophenol and pentafluorophenol) have been studied by high-resolution photofragment translational spectroscopy methods. TOF spectra of the H atom products from photolysis of 2FP and 3FP at both long (λ ~270 nm) and short (λ ~225 nm) wavelengths show structure. Only short wavelength photolysis of 26DFP and 345TFP yields structured H atom TOF spectra, while all spectra obtained from PFP were weak and devoid of structure.

Analyses of the observed structure informs on the vibrational energy disposal in the partner fluorophenoxyl radicals and how this varies with excitation wavelength, and allows estimation of (upper limits to) the respective O–H bond dissociation energies: D_0(2FPyl–H) ≤ 30220 ± 50 cm^{-1};

D_0(3FPyl–H) ≤ 29840 ± 50 cm^{-1}; D_0(26DFPyl–H) ≤ 29510 ± 50 cm^{-1}; and D_0(345TFPyl–H) ≤ 30100 ± 50 cm^{-1}. As with the phenoxyl radicals from UV photolysis of bare phenol,[7] analysis reveals that all populated product levels have overall *a″* vibrational symmetry. Typically, these involve in-plane, coupled (in- and out-of-phase) C–O and C–F wagging motions built on an odd number (usually one) quantum of an out-of-plane vibration that is assumed to be activated during non-adiabatic coupling at the relevant CI(s) en route to dissociation. The in-plane C–O/C–F wagging motions derive from the impulsive release of the H from the pendant O atom, but the relative activity in the in- and out-of-phase motions is seen to be sensitive to the presence (in 2FP and 26DFP) or absence (in 3FP or 345TFP) of the intramolecular H-bond. Again as in bare phenol, photoexcitation of specific Franck-Condon active vibronic features within the long wavelength (S_1–S_0) absorption of 2FP and 3FP tends to yield radical fragments carrying excitation in the corresponding vibrational mode of the radical product (i.e. the in-plane vibration excited in the parent, orthogonal to the O–H dissociation coordinate, tends to map through into the radical as a 'spectator').

Our inability to measure structured H atom TOF spectra when exciting 26DFP and 345TFP at long wavelengths suggests that multiple fluorination impedes tunneling from low-lying S_1 levels and/or enhances the rate of rival excited state decay pathways. Perfluorination appears to reduce the O–H bond fission probability at all wavelengths. Recent theory suggests that the latter observation, at least, may be linked to the relative lowering in energy of other C–F bond centered πσ* states that offer alternative internal conversion routes to the S_0 state. Time-resolved studies may be valuable in further elucidating the dynamics of these more fluorinated molecules.

ASSOCIATED CONTENT

Supporting Information

The Supporting Information is available free of charge at [ACS to add]

Harmonic and anharmonic normal mode wavenumbers for the ground states of the parent molecules and product radicals. TKER spectra derived from H atom TOF spectra following photolysis of 2-fluorophenol, 3-fluorophenol, 2,6-difluorophenol, and 3,4,5-trifluorophenol at all wavelengths investigated, and sample spectra for pentafluorophenol. Depictions of the vibrational modes of the product radicals assigned in the various E_{int} spectra.

Author Information

Corresponding Authors

*(MNRA) E-mail: mike.ashfold@bristol.ac.uk. Tel: +44 117 928 8312.

*(GAC) E-mail: g.cooper@missouri.edu. Tel: +1 573 289 5802

Notes

The authors declare no competing financial interest.

All underlying data are available at the University of Bristol data repository, data.bris, at [to be added post review stage]

Acknowledgements

This work was supported by the Engineering and Physical Sciences Research Council (Programme Grant EP/L005913).

References

1. Sobolewski, A. L.; Domcke, W.; Dedonder-Lardeux, C.; Jouvet, C., Excited-state Hydrogen Detachment and Hydrogen Transfer Driven by Repulsive $^1\pi\sigma^*$ States: A New Paradigm for Nonradiative Decay in Aromatic Biomolecules. *Phys. Chem. Chem. Phys.* **2002,** *4* (7), 1093-1100.
2. Tseng, C.-M.; Lee, Y. T.; Ni, C.-K.; Chang, J.-L., Photodissociation Dynamics of the Chromophores of the Amino Acid Tyrosine: p-Methylphenol, p-Ethylphenol, and p-(2-Aminoethyl)phenol. *J. Phys. Chem. A* **2007,** *111* (29), 6674-6678.
3. Iqbal, A.; Stavros, V. G., Active Participation of $^1\pi\sigma^*$ States in the Photodissociation of Tyrosine and Its Subunits. *J. Phys. Chem. Lett.* **2010,** *1* (15), 2274-2278.
4. Tomasello, G.; Wohlgemuth, M.; Petersen, J.; Mitrić, R., Photodynamics of Free and Solvated Tyrosine. *The Journal of Physical Chemistry B* **2012,** *116* (30), 8762-8770.
5. Tseng, C.-M.; Lee, Y. T.; Ni, C.-K., H Atom Elimination from the πσ* State in the Photodissociation of Phenol. *J. Chem. Phys.* **2004,** *121* (6), 2459-2461.
6. Ashfold, M. N. R.; Cronin, B.; Devine, A. L.; Dixon, R. N.; Nix, M. G. D., The Role of πσ* Excited States in the Photodissociation of Heteroaromatic Molecules. *Science* **2006,** *312* (5780), 1637-1640.
7. Nix, M. G. D.; Devine, A. L.; Cronin, B.; Dixon, R. N.; Ashfold, M. N. R., High Resolution Photofragment Translational Spectroscopy Studies of the Near Ultraviolet Photolysis of Phenol. *J. Chem. Phys.* **2006,** *125* (13), 133318.
8. Tseng, C.-M.; Lee, Y. T.; Lin, M.-F.; Ni, C.-K.; Liu, S.-Y.; Lee, Y.-P.; Xu, Z. F.; Lin, M. C., Photodissociation Dynamics of Phenol. *J. Phys. Chem. A* **2007,** *111* (38), 9463-9470.
9. Hause, M. L.; Heidi Yoon, Y.; Case, A. S.; Crim, F. F., Dynamics at Conical Intersections: The Influence of O–H Stretching Vibrations on the Photodissociation of Phenol. *J. Chem. Phys.* **2008,** *128* (10), 104307.
10. Ashfold, M. N. R.; Devine, A. L.; Dixon, R. N.; King, G. A.; Nix, M. G. D.; Oliver, T. A. A., Exploring Nuclear Motion through Conical Intersections in the UV Photodissociation of Phenols and Thiophenol. *Proc. Natl. Acad. Sci. U.S.A.* **2008,** *105* (35), 12701.
11. King, G. A.; Oliver, T. A. A.; Nix, M. G. D.; Ashfold, M. N. R., High Resolution Photofragment Translational Spectroscopy Studies of the Ultraviolet Photolysis of Phenol-d_5. *J. Phys. Chem. A* **2009,** *113* (28), 7984-7993.
12. Iqbal, A.; Cheung, M. S. Y.; Nix, M. G. D.; Stavros, V. G., Exploring the Time-Scales of H-Atom Detachment from Photoexcited Phenol-h_6 and Phenol-d_5: Statistical vs Nonstatistical Decay. *J. Phys. Chem. A* **2009,** *113* (29), 8157-8163.
13. Pino, G. A.; Oldani, A. N.; Marceca, E.; Fujii, M.; Ishiuchi, S. I.; Miyazaki, M.; Broquier, M.; Dedonder, C.; Jouvet, C., Excited State Hydrogen Transfer Dynamics in Substituted Phenols and Their Complexes with Ammonia: ππ∗-πσ∗ Energy Gap Propensity and *Ortho*-Substitution Effect. *J. Chem. Phys.* **2010,** *133* (12), 124313.
14. Dixon, R. N.; Oliver, T. A. A.; Ashfold, M. N. R., Tunnelling Under a Conical Intersection: Application to the Product Vibrational State Distributions in the UV Photodissociation of Phenols. *J. Chem. Phys.* **2011,** *134* (19), 194303.
15. Livingstone, R. A.; Thompson, J. O. F.; Iljina, M.; Donaldson, R. J.; Sussman, B. J.; Paterson, M. J.; Townsend, D., Time-Resolved Photoelectron Imaging of Excited State Relaxation Dynamics in Phenol, Catechol, Resorcinol, and Hydroquinone. *J. Chem. Phys.* **2012,** *137* (18), 184304.
16. Roberts, G. M.; Chatterley, A. S.; Young, J. D.; Stavros, V. G., Direct Observation of Hydrogen Tunneling Dynamics in Photoexcited Phenol. *J. Phys. Chem. Lett.* **2012,** *3* (3), 348-352.
17. Zhang, Y.; Oliver, T. A. A.; Ashfold, M. N. R.; Bradforth, S. E., Contrasting the Excited State Reaction Pathways of Phenol and *para*-Methylthiophenol in the Gas and Liquid Phases. *Faraday Discuss.* **2012,** *157* (0), 141-163.

18. Lai, H. Y.; Jhang, W. R.; Tseng, C.-M., Communication: Mode-Dependent Excited-State Lifetime of Phenol Under the S_1/S_2 Conical Intersection. *J. Chem. Phys.* **2018,** *149* (3), 031104.
19. Hilsabeck, K. I.; Meiser, J. L.; Sneha, M.; Harrison, J. A.; Zare, R. N., Nonresonant Photons Catalyze Photodissociation of Phenol. *J. Am. Chem. Soc.* **2019,** *141* (2), 1067-1073.
20. Woo, K. C.; Kim, S. K., Multidimensional H Atom Tunneling Dynamics of Phenol: Interplay between Vibrations and Tunneling. *J. Phys. Chem. A* **2019,** *123* (8), 1529-1537.
21. Lin, Y.-C.; Lee, C.; Lee, S.-H.; Lee, Y.-Y.; Lee, Y. T.; Tseng, C.-M.; Ni, C.-K., Excited-State Dissociation Dynamics of Phenol Studied by a New Time-Resolved Technique. *J. Chem. Phys.* **2018,** *148* (7), 074306.
22. Sobolewski, A. L.; Domcke, W., Photoinduced Electron and Proton Transfer in Phenol and Its Clusters with Water and Ammonia. *J. Phys. Chem. A* **2001,** *105* (40), 9275-9283.
23. Lan, Z.; Domcke, W.; Vallet, V.; Sobolewski, A. L.; Mahapatra, S., Time-Dependent Quantum Wave-Packet Description of the $^1\pi\sigma^*$ Photochemistry of Phenol. *J. Chem. Phys.* **2005,** *122* (22), 224315.
24. Vieuxmaire, O. P. J.; Lan, Z.; Sobolewski, A. L.; Domcke, W., *Ab Initio* Characterization of the Conical Intersections Involved in the Photochemistry of Phenol. *J. Chem. Phys.* **2008,** *129* (22), 224307.
25. Xu, X.; Yang, K. R.; Truhlar, D. G., Diabatic Molecular Orbitals, Potential Energies, and Potential Energy Surface Couplings by the 4-fold Way for Photodissociation of Phenol. *J. Chem. Theory Comput.* **2013,** *9* (8), 3612-3625.
26. Xu, X.; Zheng, J.; Yang, K. R.; Truhlar, D. G., Photodissociation Dynamics of Phenol: Multistate Trajectory Simulations including Tunneling. *J. Am. Chem. Soc.* **2014,** *136* (46), 16378-16386.
27. Yang, K. R.; Xu, X.; Zheng, J.; Truhlar, D. G., Full-Dimensional Potentials and State Couplings and Multidimensional Tunneling Calculations for the Photodissociation of Phenol. *Chem. Sci.* **2014,** *5* (12), 4661-4680.
28. Xie, C.; Ma, J.; Zhu, X.; Yarkony, D. R.; Xie, D.; Guo, H., Nonadiabatic Tunneling in Photodissociation of Phenol. *J. Am. Chem. Soc.* **2016,** *138* (25), 7828-7831.
29. Zhu, X.; Yarkony, D. R., On the Elimination of the Electronic Structure Bottleneck in On the Fly Nonadiabatic Dynamics for Small to Moderate Sized (10-15 Atom) Molecules Using Fit Diabatic Representations Based Solely on Ab Initio Electronic Structure Data: The Photodissociation of Phenol. *J. Chem. Phys.* **2016,** *144* (2), 024105.
30. Xie, C.; Guo, H., Photodissociation of Phenol via Nonadiabatic Tunneling: Comparison of Two Ab Initio Based Potential Energy Surfaces. *Chem. Phys. Lett.* **2017,** *683*, 222-227.
31. Xie, W.; Domcke, W., Accuracy of Trajectory Surface-Hopping Methods: Test for a Two-Dimensional Model of the Photodissociation of Phenol. *J. Chem. Phys.* **2017,** *147* (18), 184114.
32. He, Y.; Zhao, H.; Wang, W., Photodissociation of Phenol in the Adiabatic Representation: Tunneling, Motions of Phenyl Ring, and Kinetic Isotope Effects. *Int. J. Quantum Chem.* **2018,** *118* (24), e25786.
33. Xie, C.; Zhao, B.; Malbon, C. L.; Yarkony, D. R.; Xie, D.; Guo, H., Insights into the Mechanism of Nonadiabatic Photodissociation from Product Vibrational Distributions. The Remarkable Case of Phenol. *J. Phys. Chem. Lett.* **2020,** *11* (1), 191-198.
34. Devine, A. L.; Nix, M. G. D.; Cronin, B.; Ashfold, M. N. R., Near-UV Photolysis of Substituted Phenols, I: 4-Fluoro-, 4-Chloro- and 4-Bromophenol. *Phys. Chem. Chem. Phys.* **2007,** *9* (28), 3749-3762.
35. Hadden, D. J.; Roberts, G. M.; Karsili, T. N. V.; Ashfold, M. N. R.; Stavros, V. G., Competing $^1\pi\sigma^*$ Mediated Dynamics in Mequinol: O–H *Versus* O–CH3 Photodissociation Pathways. *Phys. Chem. Chem. Phys.* **2012,** *14* (38), 13415-13428.
36. Chatterley, A. S.; Young, J. D.; Townsend, D.; Żurek, J. M.; Paterson, M. J.; Roberts, G. M.; Stavros, V. G., Manipulating Dynamics with Chemical Structure: Probing Vibrationally-Enhanced Tunnelling in Photoexcited Catechol. *Phys. Chem. Chem. Phys.* **2013,** *15* (18), 6879-6892.

37. Karsili, T. N. V.; Wenge, A. M.; Harris, S. J.; Murdock, D.; Harvey, J. N.; Dixon, R. N.; Ashfold, M. N. R., O–H Bond Fission in 4-Substituted Phenols: S_1 State Predissociation Viewed in a Hammett-like Framework. *Chem. Sci.* **2013,** *4* (6), 2434-2446.
38. Sage, A. G.; Oliver, T. A. A.; King, G. A.; Murdock, D.; Harvey, J. N.; Ashfold, M. N. R., UV Photolysis of 4-Iodo-, 4-Bromo-, and 4-Chlorophenol: Competition Between C–Y (Y = Halogen) and O–H Bond Fission. *J. Chem. Phys.* **2013,** *138* (16), 164318.
39. Karsili, T. N. V.; Wenge, A. M.; Marchetti, B.; Ashfold, M. N. R., Symmetry Matters: Photodissociation Dynamics of Symmetrically Versus Asymmetrically Substituted Phenols. *Phys. Chem. Chem. Phys.* **2014,** *16* (2), 588-598.
40. Harris, S. J.; Karsili, T. N. V.; Murdock, D.; Oliver, T. A. A.; Wenge, A. M.; Zaouris, D. K.; Ashfold, M. N. R.; Harvey, J. N.; Few, J. D.; Gowrie, S.; *et al*., A Multipronged Comparative Study of the Ultraviolet Photochemistry of 2-, 3-, and 4-Chlorophenol in the Gas Phase. *J. Phys. Chem. A* **2015,** *119* (23), 6045-6056.
41. Brundle, C. R.; Robin, M. B.; Kuebler, N. A., Perfluoro Effect in Photoelectron Spectroscopy. II. Aromatic Molecules. *J. Am. Chem. Soc.* **1972,** *94* (5), 1466-1475.
42. Philis, J.; Bolovinos, A.; Andritsopoulos, G.; Pantos, E.; Tsekeris, P., A Comparison of the Absorption Spectra of the Fluorobenzenes and Benzene in the Region 4.5-9.5 eV. *J. Phys. B* **1981,** *14* (19), 3621-3635.
43. Zgierski, M. Z.; Fujiwara, T.; Lim, E. C., Photophysics of Aromatic Molecules with Low-Lying πσ* States: Fluorinated Benzenes. *J. Chem. Phys.* **2005,** *122* (14), 144312.
44. Han, J.; Tao, F.-M., Correlations and Predictions of pKa Values of Fluorophenols and Bromophenols Using Hydrogen-Bonded Complexes with Ammonia. *J. Phys. Chem. A* **2006,** *110* (1), 257-263.
45. Karmakar, S.; Mukhopadhyay, D. P.; Chakraborty, T., Electronic Spectra and Excited State Dynamics of Pentafluorophenol: Effects of Low-Lying πσ∗ States. *J. Chem. Phys.* **2015,** *142* (18), 184303.
46. Rajak, K.; Ghosh, A.; Mahapatra, S., Photophysics of Phenol and Pentafluorophenol: The Role of Nonadiabaticity in the Optical Transition to the Lowest Bright $^1\pi\pi^*$ State. *J. Chem. Phys.* **2018,** *148* (5), 054301.
47. Cronin, B.; Nix, M. G. D.; Qadiri, R. H.; Ashfold, M. N. R., High Resolution Photofragment Translational Spectroscopy Studies of the Near Ultraviolet Photolysis of Pyrrole. *Phys. Chem. Chem. Phys.* **2004,** *6* (21), 5031-5041.
48. Ingle, R. A.; Karsili, T. N. V.; Dennis, G. J.; Staniforth, M.; Stavros, V. G.; Ashfold, M. N. R., Extreme Population Inversion in the Fragments Formed by UV Photoinduced S-H Bond Fission in 2-Thiophenethiol. *Phys. Chem. Chem. Phys.* **2016,** *18* (16), 11401-11410.
49. Wilson, S. H. S.; Howe, J. D.; Ashfold, M. N. R., On the Near Ultraviolet Photodissociation of Hydrogen Sulphide. *Mol. Phys.* **1996,** *88* (3), 841-858.
50. Hohenberg, P.; Kohn, W., Inhomogeneous Electron Gas. *Phys. Rev.* **1964,** *136* (3B), B864-B871.
51. Kohn, W.; Sham, L. J., Self-Consistent Equations Including Exchange and Correlation Effects. *Phys. Rev.* **1965,** *140* (4A), A1133-A1138.
52. Becke, A. D., Density-Functional Thermochemistry. III. The Role of Exact Exchange. *J. Chem. Phys.* **1993,** *98* (7), 5648-5652.
53. Lee, C.; Yang, W.; Parr, R. G., Development of the Colle-Salvetti Correlation-Energy Formula into a Functional of the Electron Density. *Phys. Rev. B* **1988,** *37* (2), 785-789.
54. Miehlich, B.; Savin, A.; Stoll, H.; Preuss, H., Results Obtained with the Correlation Energy Density Functionals of Becke and Lee, Yang and Parr. *Chem. Phys. Lett.* **1989,** *157* (3), 200-206.
55. Dunning Jr., T. H., Gaussian Basis Sets for Use in Correlated Molecular Calculations. I. The Atoms Boron through Neon and Hydrogen. *J. Chem. Phys.* **1989,** *90* (2), 1007-1023.

56. Kendall, R. A.; Dunning Jr., T. H.; Harrison, R. J., Electron Affinities of the First-Row Atoms Revisited. Systematic Basis Sets and Wave Functions. *J. Chem. Phys.* **1992,** *96* (9), 6796-6806.
57. Woon, D. E.; Dunning Jr., T. H., Gaussian Basis Sets for Use in Correlated Molecular Calculations. III. The Atoms Aluminum Through Argon. *J. Chem. Phys.* **1993,** *98* (2), 1358-1371.
58. Grimme, S.; Ehrlich, S.; Goerigk, L., Effect of the Damping Function in Dispersion Corrected Density Functional Theory. *J. Comput. Chem.* **2011,** *32* (7), 1456-1465.
59. Frisch, M. J. T., G. W.; Schlegel, H. B.; Scuseria, G. E.; Robb, M. A.; Cheeseman, J. R.; Scalmani, G.; Barone, V.; Mennucci, B.; Petersson, G. A.; et al. *Gaussian 09*, revision D.01; Gaussian, Inc.: Wallingford, CT, 2013.
60. Ratzer, C.; Küpper, J.; Spangenberg, D.; Schmitt, M., The Structure of Phenol in the S_1-State Determined by High Resolution UV-Spectroscopy. *Chem. Phys.* **2002,** *283* (1), 153-169.
61. Deng, X.; Tang, Y.; Song, X.; Liu, K.; Gu, Z.; Zhang, B., Photolysis Dynamics of m- and o-Fluorophenol: Substitution Effects on Tunneling Mechanism. *Chemosphere* **2020,** *253*, 126747.
62. Cooper, G. A.; Hansen, C. S.; Karsili, T. N. V.; Ashfold, M. N. R., Photofragment Translational Spectroscopy Studies of H Atom Loss Following Ultraviolet Photoexcitation of Methimazole in the Gas Phase. *J. Phys. Chem. A* **2018,** *122* (51), 9869-9878.
63. Devine, A. L.; Cronin, B.; Nix, M. G. D.; Ashfold, M. N. R., High Resolution Photofragment Translational Spectroscopy Studies of the Near Ultraviolet Photolysis of Imidazole. *J. Chem. Phys.* **2006,** *125* (18), 184302.
64. King, G. A.; Devine, A. L.; Nix, M. G. D.; Kelly, D. E.; Ashfold, M. N. R., Near-UV photolysis of substituted phenols Part II. 4-, 3- and 2-methylphenol. *Phys. Chem. Chem. Phys.* **2008,** *10* (42), 6417-6429.
65. Fujimaki, E.; Fujii, A.; Ebata, T.; Mikami, N., Autoionization-Detected Infrared Spectroscopy of Intramolecular Hydrogen Bonds in Aromatic Cations. I. Principle and Application to Fluorophenol and Methoxyphenol. *J. Chem. Phys.* **1999,** *110* (9), 4238-4247.
66. Moreira, M. A.; Cormanich, R. A.; de Rezende, F. M. P.; Silla, J. M.; Tormena, C. F.; Rittner, R.; Ramalho, T. C.; Freitas, M. P., Theoretical and Infrared Studies on the Conformations of Monofluorophenols. *J. Mol. Struct.* **2012,** *1009*, 11-15.
67. Kierspel, T.; Horke, D. A.; Chang, Y.-P.; Küpper, J., Spatially Separated Polar Samples of the *Cis* and *Trans* Conformers of 3-Fluorophenol. *Chem. Phys. Lett.* **2014,** *591*, 130-132.
68. Bell, A.; Singer, J.; Desmond, D.; Mahassneh, O.; van Wijngaarden, J., Rotational Spectra and Conformer Geometries of 2-Fluorophenol and 3-Fluorophenol. *J. Mol. Spectrosc.* **2017,** *331*, 53-59.
69. Wilson, E. B., The Normal Modes and Frequencies of Vibration of the Regular Plane Hexagon Model of the Benzene Molecule. *Phys. Rev.* **1934,** *45* (10), 706-714.
70. Herzberg, G., *Molecular Spectra and Molecular Structure: II Infrared and Raman Spectra of Polyatomic Molecules*. D. Van Nostrand Company, Inc.: Princeton, 1945.
71. Abraham, M. H.; Abraham, R. J.; Aliev, A. E.; Tormena, C. F., Is there an Intramolecular Hydrogen Bond in 2-Halophenols? A Theoretical and Spectroscopic Investigation. *Phys. Chem. Chem. Phys.* **2015,** *17* (38), 25151-25159.
72. Cormanich, R. A.; Moreira, M. A.; Freitas, M. P.; Ramalho, T. C.; Anconi, C. P. A.; Rittner, R.; Contreras, R. H.; Tormena, C. F., $^{1h}J_{FH}$ Coupling in 2-Fluorophenol Revisited: Is Intramolecular Hydrogen Bond Responsible for this Long-Range Coupling? *Magnetic Resonance in Chemistry* **2011,** *49* (12), 763-767.
73. Kovács, A.; Macsári, I.; Hargittai, I., Intramolecular Hydrogen Bonding in Fluorophenol Derivatives: 2-Fluorophenol, 2,6-Difluorophenol, and 2,3,5,6-Tetrafluorohydroquinone. *J. Phys. Chem. A* **1999,** *103* (16), 3110-3114.
74. Kovács, A.; Szabó, A.; Hargittai, I., Structural Characteristics of Intramolecular Hydrogen Bonding in Benzene Derivatives. *Accounts of Chemical Research* **2002,** *35* (10), 887-894.

75. Zeoly, L. A.; Coelho, F.; Cormanich, R. A., Intramolecular H-Bond Is Formed in 2-Fluorophenol and 2-Fluorothiophenol, but It May Not Be the Main Pathway of the J_{FH} Coupling Constant Transmission. *J. Phys. Chem. A* **2019,** *123* (46), 10072-10078.
76. Rosenberg, R. E.; Chapman, B. K.; Ferrill, R. N.; Jung, E. S.; Samaan, C. A., Approximating the Strength of the Intramolecular Hydrogen Bond in 2-Fluorophenol and Related Compounds: A New Application of a Classic Technique. *J. Phys. Chem. A* **2020,** *124* (19), 3851-3858.
77. John, U.; Kuriakose, S.; Nair, K. P. R., Vibrational Overtone Spectra of o-Fluorophenol and the "Anomalous" Order of Intramolecular Hydrogen Bonding Strengths. *Spectrochim. Acta A* **2007,** *68* (2), 331-336.
78. Oswald, I. D. H.; Allan, D. R.; Motherwell, W. D. S.; Parsons, S., Structures of the Monofluoro- and Monochlorophenols at Low Temperature and High Pressure. *Acta Crystallographica Section B* **2005,** *61* (1), 69-79.
79. Carlson, G. L.; Fateley, W. G.; Manocha, A. S.; Bentley, F. F., Torsional Frequencies and Enthalpies of Intramolecular Hydrogen Bonds of *o*-Halophenols. *The Journal of Physical Chemistry* **1972,** *76* (11), 1553-1557.
80. Oikawa, A.; Abe, H.; Mikami, N.; Ito, M., Electronic Spectra and Ionization Potentials of Rotational Isomers of Several Disubstituted Benzenes. *Chem. Phys. Lett.* **1985,** *116* (1), 50-54.
81. Shin, D. N.; Hahn, J. W.; Jung, K.-H.; Ha, T.-K., Study of the Cis and Trans Conformers of 2-Halophenols Using Coherent anti-Stokes Raman Spectroscopic and Quantum Chemical Methods. *Journal of Raman Spectroscopy* **1998,** *29* (4), 245-249.
82. Remmers, K.; Meerts, W. L.; Zehnacker-Rentien, A.; Le Barbu, K.; Lahmani, F., Structural Information on the S_0 and S_1 State of *o*-Fluorophenol by Hole Burning and High Resolution Ultraviolet Spectroscopy. *J. Chem. Phys.* **2000,** *112* (14), 6237-6244.
83. Yuan, L.; Li, C.; Lin, J. L.; Yang, S. C.; Tzeng, W. B., Mass Analyzed Threshold Ionization Spectroscopy of *o*-Fluorophenol and *o*-Methoxyphenol Cations and Influence of the Nature and Relative Location of Substituents. *Chem. Phys.* **2006,** *323* (2), 429-438.
84. Song, X.; Toldo, J. M.; de Moura, C. E. V.; Tang, Y.; Zhang, B.; Barbatti, M., Photodissociation Dynamics of Ortho and Meta Fluorophenols: The Origin of Fast Protons. ChemRxiv Preprint, 2020.

TOC Figure